Original Article

Institution of MECHANICAL ENGINEERS
Journal of ENGINEERING TRIBOLOGY

Proc IMechE Part J:
J Engineering Tribology
0(0) 1–17

DOI: 10.1177/1350650117727230
journals.sagepub.com/home/pij
SAGE

Dynamic modeling of an eccentric face seal including coupled rotordynamics, face contact, and inertial maneuver loads

Philip Varney[1] and Itzhak Green[2]

Abstract

Mechanical face seals are constitutive components of turbomachines, which in turn can be constitutive to other systems (e.g. aircraft). Furthermore, the rotating element of a face seal is inextricably coupled to the turbomachine via a flexible mount, and the stationary seal element is coupled to the rotating seal element via the fluid film existing between the seal faces. Consequentially, understanding interactions between the seal and turbomachine is important for quantifying seal performance and improving its design. With few exceptions, previous works study the face seal dynamics independent from the rotordynamics. In addition, most prior investigations consider only angular and axial seal dynamics and neglect eccentric (i.e. lateral) deflections of the seal element(s). For the first time, this work develops a comprehensive and novel model of a mechanical face seal in the inertial reference frame including coupled rotordynamics and inertial maneuver loads of the overall system. The model is developed for a general seal geometry where both seal elements, stationary and rotating, are flexibly mounted and allowed to undergo angular, axial, and eccentric deflections. In addition, the seal model presented here accounts for transient operation, fluid shear forces, seal face contact, friction, and thermoelastic deformation. Finally, various faults due to manufacturing imperfections, component flaws, and/or installation errors can be accounted for by incorporating static angular misalignment of both seal elements, dynamic angular misalignment of the rotating seal element, eccentric rotating imbalance, and axial offset of the rotating seal element center of mass. Throughout this work, the equations of motion developed are valid for both steady-state and transient operation. This comprehensive model significantly advances the state of the art in mechanical face seal dynamic modeling and represents a pivotal step towards analyzing seal performance regarding a broad diversity of realistic problems.

Keywords

Rotordynamics, mechanical face seals, dynamics, vibrations, rough surface contact, impact, nonlinear dynamics

Date received: 14 November 2016; accepted: 8 July 2017

Introduction

Mechanical face seals allow a rotating shaft to transfer power through fluid reservoirs of differing pressure. The seal apparatus is classified according to which element, rotating or stationary, is flexibly mounted (e.g. flexibly mounted stator (FMS), flexibly mounted rotor (FMR), or flexibly mounted stator-rotor (FMSR) seals). It is important to note that designating the rotating seal element as the rotor is vestigial from previous works that negated the rotordynamics. In this work, the 'rotor' refers to the flexible shaft and rigid disc(s) of the complete turbomachine. Mechanical face seals are also categorized according to how fluid sealing is generated. Contacting mechanical face seals rely primarily on seal face asperity contact to provide sealing and restrict leakage. Unfortunately, the useful life of this design is limited by friction, wear, and excessive thermal deformation, and the element must be routinely repaired or replaced. On the other hand, non-contacting mechanical face seals, such as those considered in this work, create fluid sealing via hydrostatic and/or hydrodynamic pressure; this design extends the element's useful life at the expense of increased fluid leakage.[1,2]

Understanding how mechanical face seals and turbomachines interact is paramount towards developing the next generation of high-performance mechanical

[1]Pratt & Whitney, East Hartford, CT, USA
[2]Woodruff School of Mechanical Engineering, Georgia Institute of Technology, Atlanta, GA, USA

Corresponding author:
Philip Varney, Pratt & Whitney, 400 Main St., East Hartford, CT 06118, USA.
Email: phil.a.varney@gmail.com

face seals. Because non-contacting mechanical face seals reduce friction and increase component life, they are often used in high-performance applications such as nuclear reactor coolant pumps and high-speed turbomachinery.[3] Increased turbomachine efficiencies are often achieved by reducing fluid clearances, increasing rotor shaft speeds, and implementing lighter and more flexible rotors; these enhancements undoubtedly influence seal performance. Greater shaft speeds and lighter, more flexible rotors increase rotor vibration, while smaller fluid-film clearances increase the chance for undesirable seal face contact. One study indicates that reducing turbomachine fluid clearances in a broad array of industries could save 1.554 billion gallons of fossil fuels consumed annually (i.e. 0.3% of the U.S. energy consumption[4]). Mechanical face seal designs must advance commensurately with modern turbomachinery improvements, thus requiring unified dynamic models of the coupled turbomachine-seal system.

The objective of a non-contacting mechanical face seal is to minimize leakage while avoiding face contact; both of these concerns are dictated by the seal face dynamics. Face seal dynamics have been extensively studied for the case where the rotordynamics are neglected. The seal dynamics are predicated on modeling the forces developed within the fluid sealing dam. Etsion et al.[5–7] derive the fluid pressure within a narrow seal[8] and include hydrostatic, hydrodynamic, and squeeze effects. The fluid pressure is then applied to obtain the fluid film forces and moments (and associated stiffness and damping coefficients) for an FMS mechanical face seal.[9] These forces and moments (or, equivalently, the linearized rotordynamic coefficients) are instituted in the seal equations of motion to predict the angular response versus static misalignment of the rotating seal element.[10,11] Similar analyses have also been performed for an FMR configuration,[12–14] where, once again, the designation 'rotor' is a vestigial moniker referring to the rotating seal element. Lee and Green[15] construct a test rig and experimentally verify the results of the FMR model by extracting the seal's dynamic response using a suite of eddy-current proximity probes.

The dynamics of a seal where both elements are free to deflect has also been previously studied. Once again, recall that the term 'rotor' in the following studies refers to a rotating seal element and not the turbomachine rotor. Wileman and Green[16,17] develop the equations of motion for an FMRR seal where both elements are permitted to rotate. Even though the FMRR configuration is uncommon in practice, it represents the most generic case and can be degenerated into any of the more common seal configurations. Results from a later analysis[18] discuss performance differences between FMS, FMR and FMSR seal configurations. The FMR and FMSR configurations both produce smaller relative misalignments than an FMS configuration. The model is later expanded to include eccentric deflections,[19] where preliminary results are found by assuming constant synchronous shaft whirl.[20] The eccentric fluid film forces used therein are based on previous derivations by Etsion[21] for eccentric misaligned face seals.

Excessive rotor vibration can precipitate intermittent face contact in mechanical seals. Etsion and Constantinescu[22] encounter face contact in an FMS seal test rig, and suggest contact as a possible explanation for seal failure. Lee and Green[15,23] also observe unexpected face contact in an experimental seal test rig, and subsequently employ a heuristic approach for quantifying contact-induced higher harmonic oscillations. Varney and Green[24] use asperity contact models to simulate intermittent face contact in a non-contacting mechanical seal. The simulation results from their study validate previously observed contact vibration signatures. Etsion and Halperin[25] suggest using laser surface texturing to increase the stiffness of the fluid film, thereby reducing the propensity for face contact. A comprehensive transient analysis is conducted by Green[26] that seamlessly accounts for the transition between contacting and non-contacting states of operation, where the model includes surface roughness, start-up/shut-down operation, and thermoelastic face coning. In a similar study, Wang et al.[27] use a more complex thermoelastic mechanical seal model to investigate local variations in deformation and temperature across the seal surfaces. Valigi et al.[28] perform a parametric analysis to ascertain the impact of instabilities and stick-slip friction in the transient performance of a mechanical face seal. Still, none of these works attempt to quantify the influence of rotordynamics on seal dynamic performance.

The few works that include rotordynamics in existing seal models indicate that the rotor does indeed influence the seal dynamics. Lee and Green[29] use the transfer matrix method and linearized fluid film coefficients to couple the shaft rotordynamics and FMR seal dynamics, and use the results to eliminate rotordynamic effects as an explanation for unexplained vibrations in a mechanical seal test rig. Still, results from their study indicate that the rotordynamics do indeed influence seal performance when the rotor is sufficiently flexible. Varney and Green[30] incorporate angular rotordynamics into the transient performance of an FMS seal and show that passage through the rotor critical speed provokes undesirable face contact. The effect of machine vibration is discussed by Green,[31] where machine vibration is integrated into an FMS seal dynamic analysis by imposing a white noise perturbation in the axial film thickness equation.

The objective of this work is to develop, for the first time, a novel comprehensive model for an FMSR seal including both eccentric deflections and external coupled rotordynamics. This seal model will be referred to as the FMSR-ER seal, where the

modifiers indicate that eccentric deflections and coupled rotordynamic effects have been considered. Specifically, this model represents a comprehensive approach to model mechanical face seal dynamics by including the following effects:

1. Coupled rotordynamic effects of the turbomachine.
2. Inertial maneuver loads of the supporting structure, including translation and rotation.
3. Transient and steady-state operation of the system allowing for start-up and shut-down regimes.
4. Static and dynamic angular misalignment.
5. Lateral and axial mass imbalance.
6. Fluid pressure for an isoviscous, isothermal, and incompressible fluid, including fluid shear forces.
7. Contact pressure and friction found from the elasto-plastic Jackson-Green rough surface contact model.[24,32,33]
8. Thermoelastic deformation caused by viscous and frictional heat generation.

This complete model represents a significant step forward in describing and understanding the dynamic performance of non-contacting mechanical face seals and provides a useful tool for studying the holistic performance of mechanical face seal systems.

A kinematic description of the FMSR seal

The FMSR-ER mechanical face seal with a flexible shaft and riding disc is shown in Figure 1. The stationary seal element is an annular ring mounted to the housing using an axial support spring and a secondary seal O-ring. Rotation of both seal elements about the shaft axis is constrained by an anti-rotation lock[14,34] (i.e. torsional dynamics are neglected herein). Opposite to the stationary seal element is the flat-faced seal seat, which in this work is the rotating element. The rotating seal element is affixed to a disc and flexible shaft (i.e. the rotor). A thin fluid film separates the stationary and rotating seal elements, where the region between the elements is referred to as the sealing dam. Face coning and relative deflections induce hydrostatic and hydrodynamic fluid forces, which in turn generate clearances sufficient for (hopefully) avoiding undesirable face contact. The seal is balanced so that the opening and closing forces are equivalent during operation, thus providing a desired set-point clearance C_o between the stationary and rotating seal faces. Given a prescribed inner and outer pressure (P_i and P_o), the magnitude of C_o is found by appropriately selecting the support spring stiffness F_{spr} along with the inner, outer, and balance radii (r_i, r_o, and r_b, respectively).[26]

Degrees of freedom

The stationary and rotating seal elements are permitted to translate axially, deflect eccentrically, and rotate about axes orthogonal to the axis of rotation. The positive-drive devices (e.g. anti-rotation locks) constrain torsional deflections of both elements, and thus, this work does not consider torsional dynamics. Thus, the dynamics of each seal element are described using five degrees of freedom, and the total seal apparatus (i.e. the FMSR-ER) constitutes a 10 degree-of-freedom dynamic system. Here, the symbols u, ϵ, and γ are used to denote axial deflection,

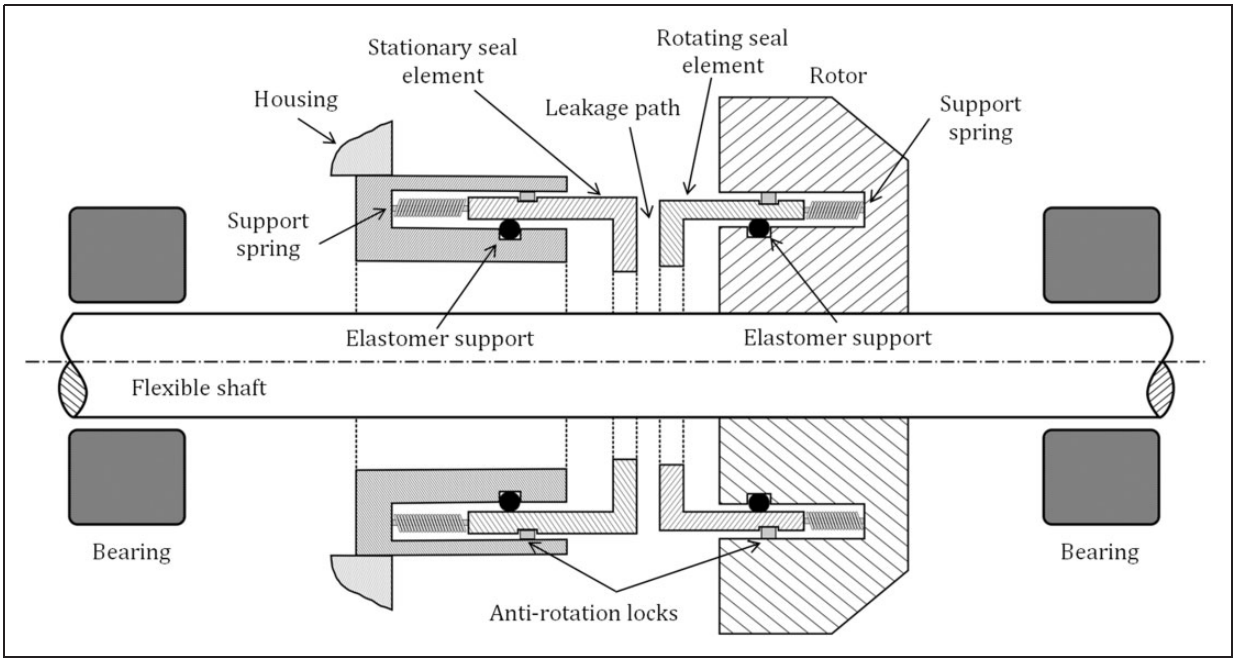

Figure 1. FMSR-ER seal apparatus showing the coupled rotor (i.e. the flexible shaft riding disc).

eccentric deflection, and tilt, respectively. The first subscript on each degree-of-freedom signifies the seal element ('r' for the rotating element and 's' for the stationary element). The second subscript signifies direction. In vector form, the degrees-of-freedom including time-dependent thermal coning $\beta(t)$ are

$$\{q\} = \{\gamma_{s\xi} \quad \gamma_{s\eta} \quad u_{sz} \quad \epsilon_{s\xi} \quad \epsilon_{s\eta} \quad \gamma_{r\xi} \quad \gamma_{r\xi} \quad u_{rz} \quad \epsilon_{r\xi} \quad \epsilon_{r\eta} \quad \beta\}^T \tag{1}$$

This vector can be expanded to include any number of rotor degrees-of-freedom, if the seal dynamics must be solved commensurately to the rotordynamics. As will be seen, the seal elements are fundamentally coupled by a thin fluid film (and possibly contact) between the seal faces. In addition, the rotating seal element dynamics are inextricably coupled to those of the rotor for practical seal/rotor systems, although the converse depends on whether the rotor is significantly larger than the seal.

Reference frames

A necessary prerequisite for understanding the system kinematics and dynamics is understanding the reference frames used to describe the dynamics of each seal element. These reference frames are shown in Figure 2 for both seal elements. The reference frames of interest here are:

1. $\xi\eta\zeta$: A system-fixed (e.g. turbomachine-fixed) reference frame attached to the concentric undeflected location of rotating seal element geometric center, O_r (the stationary element geometric center O_s is separated from O_r by the fixed nominal clearance C_o). The acceleration of this point is $\bar{a}_O$, and the frame rotates with angular velocity $\bar{\lambda}_0$. The acceleration $\bar{a}_O$ and rotation rate $\bar{\lambda}_0$ constitute the inertial maneuver of the overall structure. This frame is inertial if system maneuver is neglected.
2. $\xi_s\eta_s\zeta_s$: A system-fixed reference frame attached to the stationary seal element geometric center, C_s. This frame also experiences the maneuver rates associated with $\bar{a}_O$ and $\bar{\lambda}_0$.
3. $X_sY_sZ_s$: This frame is precessed about ζ_s by the precession ψ_s. X_s defines the axis about which the stationary seal element nutates (i.e. tilts).
4. $x_sy_sz_s$: This principal frame is nutated about X_s by γ_s.
5. $\xi_r\eta_r\zeta_r$: A system-fixed reference frame attached to the rotating seal element geometric center, C_r. This frame also experiences the maneuver loads caused by $\bar{a}_O$ and $\bar{\lambda}_0$. The axis ζ_r defines the direction of shaft rotation.
6. $X'_rY'_rZ'_r$: This frame is precessed about ζ_r by the shaft rotation angle $\alpha(t)$, which is related to the shaft speed ω_r

$$\alpha(t) = \int_0^t \omega_r(t')\mathrm{d}t' \tag{2}$$

7. $X_rY_rZ_r$: This frame is precessed about ζ_r by the absolute rotating seal element precession ψ_r, or alternatively, precessed about Z'_r by the relative precession ψ' (i.e. $\psi_r = \alpha(t) + \psi'$).
8. $x_ry_rz_r$: This frame is nutated about X_r by γ_r.
9. $1_r2_r3_r$: This body-fixed, but not necessarily principal, frame is obtained by applying spin ϕ about z_r. The spin ϕ is related to the relative precession ψ' by $\dot{\phi} = -\dot{\psi}'$[14,34]
10. $x^p_ry^p_rz^p_r$: This frame is rotated about 1_r by the dynamic angular misalignment χ and represents a body-fixed set of principal axes for the rotating seal element. The dynamic angular misalignment χ defines the angle between the body-fixed spinning reference frame $(123)_r$ and the principal frame.

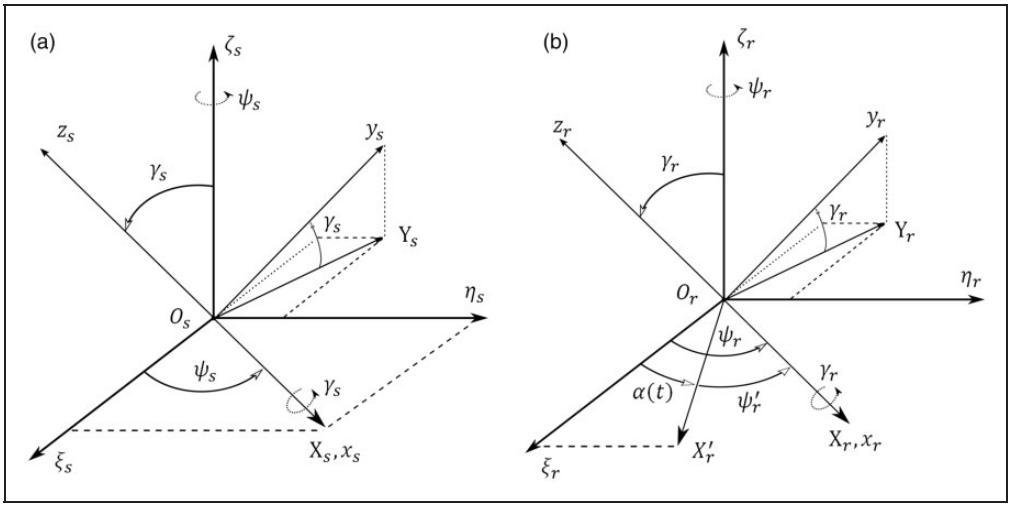

Figure 2. Reference frames used to describe the angular kinematics of the stationary and rotating seal elements. (a) Flexibly mounted stationary seal element and (b) flexibly mounted rotating seal element.

Inertial maneuver profile

The overall system (e.g. turbojet or turbofan engine) accelerates at $\bar{a}_O$ and rotates at $\bar{\lambda}_0$. In component form, the system acceleration is

$$\bar{a}_O = a_{O\xi}\hat{e}_\xi + a_{O\eta}\hat{e}_\eta + a_{O\zeta}\hat{e}_\zeta \tag{3}$$

The system can also experience rotations in addition to translations. The components of the maneuver rotation relative to $\xi\eta\zeta$ are referred to here as pitch, yaw, and roll, respectively. The maneuver angular velocity $\bar{\lambda}_0$ is then written in the following form

$$\bar{\lambda}_0 = \lambda_p\hat{e}_\xi + \lambda_y\hat{e}_\eta + \lambda_{ro}\hat{e}_\zeta \tag{4}$$

where the magnitudes of the pitch, yaw, and roll angular velocities are λ_p, λ_y, and λ_{ro}, respectively, and are functions of time which also may depend on the orientation of the overall structure. To remain consistent with previous seal dynamics literature,[34] equation (4) is transformed into the rotating $x_r y_r z_r$ frame

$$\begin{aligned}\bar{\lambda}_0 = {} & (\lambda_p \cos\psi_r + \lambda_y \sin\psi_r)\hat{e}_{x_r} \\ & + (\gamma_r\lambda_{ro} + \lambda_y \cos\psi_r - \lambda_p \sin\psi_r)\hat{e}_{y_r} \\ & + (\lambda_{ro} - \gamma_r\lambda_y \cos\psi_r + \lambda_p \sin\psi_r)\hat{e}_{z_r}\end{aligned} \tag{5}$$

Eccentric kinematics

Both seal elements are permitted to deflect laterally (i.e. eccentrically). To remain consistent with prior seal dynamics nomenclature, these lateral deflections will be referred to as eccentricities (not to be confused with lateral imbalance of the center of mass). The eccentric kinematic analysis is performed in the system-fixed $\xi\eta\zeta$ frame because (a) condition monitoring systems usually measure inertial dynamics and (b) the contact reactions will be easier to intuit in the system-fixed frame. The consequence of choosing a system-fixed versus rotating frame is somewhat arbitrary, since other phenomena (e.g. shaft cracks) are easier to understand in a shaft-fixed rotating frame. Nevertheless, a choice must be made, and the system-fixed frame will be employed herein.

The eccentric kinematics for the stationary and rotating seal elements are shown in Figure 3(a). The geometric centers of the stationary and rotating seal elements are denoted C_s and C_r, respectively. The undeflected geometric centers of both elements lie at O_s and O_r along the shaft rotation axis; in this work, these points are assumed to be co-linear. The eccentric deflection of element j in the ith direction is labeled ϵ_{ji}. Using the inertial $\xi\eta\zeta$ frame, the planar position vectors locating the center of each element with respect to $O_{r,s}$ are

$$\bar{r}_{(CO)_s} = \epsilon_{s\xi}\hat{e}_\xi + \epsilon_{s\eta}\hat{e}_\eta \tag{6}$$

$$\bar{r}_{(CO)_r} = \epsilon_{r\xi}\hat{e}_\xi + \epsilon_{r\eta}\hat{e}_\eta \tag{7}$$

As will be seen, friction forces and fluid shear forces depend on the relative eccentricity between the elements and the relative eccentric velocity. From Figure 3(a), the relative eccentricity vector is

$$\bar{\epsilon}^* = \bar{r}_{(CO)_s} - \bar{r}_{(CO)_r} \tag{8}$$

The dynamic forces are functions of the acceleration of each element's center of mass. This work assumes that the stationary seal element is

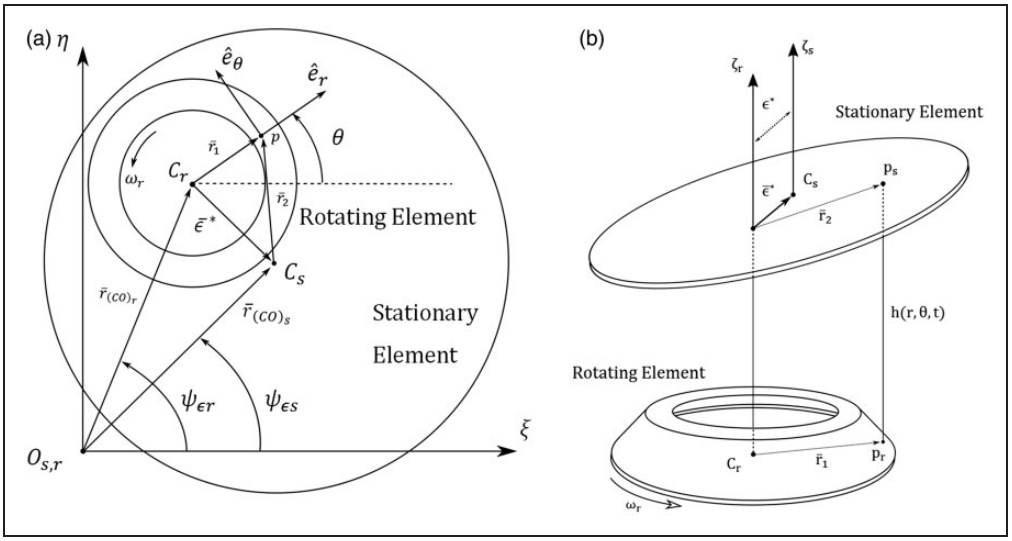

Figure 3. Eccentric deflections of the stationary and rotating seal elements. (a) Planar kinematics of seal eccentricity and (b) film thickness at a corresponding point on each surface.

eccentrically balanced, that is $C_s = G_s$; consequently, the acceleration of the stationary element center of mass relative to C_s is found by differentiating equation (6)

$$\bar{a}_{G_s} = \bar{a}_{C_s} = \bar{a}_o + \frac{\partial^2 \bar{r}_{(CO)_s}}{\partial t^2} + \dot{\bar{\lambda}}_0 \times \bar{r}_{(CO)_s} + \bar{\lambda}_0 \times \bar{\lambda}_0 \times \bar{r}_{(CO)_s} + 2\bar{\lambda}_0 \times \frac{\partial \bar{r}_{(CO)_s}}{\partial t} \tag{9}$$

where $\bar{\lambda}_0$ is the maneuver rotation of the system, and thus, the system-fixed frame rotation rate.

Expressing the rotating seal element center of mass acceleration is complicated by imbalance, axial offset, and shaft rotation; these parameters are shown in Figure 4(a) and (b). The center of mass G_r is laterally offset from C_r by the eccentric imbalance ε_{rG}, occurring at an angle β_r from the body-fixed spin axis 1_r. Furthermore, G_r is axially offset from C_r by the distance d_r. The following position vector locates the center of mass relative to the geometric center using the body-fixed stationary seal element spin axes $(xyz)_r^p$

$$\bar{r}_{(CG)_r} = \varepsilon_{rG} \cos\beta_r \hat{e}_{x_r^p} + \varepsilon_{rG} \sin\beta_r \hat{e}_{y_r^p} + d_r \hat{e}_{z_r^p} \tag{10}$$

where β_r is the static phase angle locating G_r in the $x_r^p y_r^p$ plane (referenced from x_r^p). The body-fixed frame is convenient to use because the imbalance and offset are body-fixed quantities. The position vectors $\bar{r}_{(CG)_r}$ and $\bar{r}_{(CO)_r}$ must be written relative to the same frame before calculating the acceleration of G_r

$$\bar{r}_{(CG)_r}|^{\xi\eta\zeta} = [R_r]^T \bar{r}_{(CG)_r}|^{(xyz)_r^p} \tag{11}$$

where

$$[R_r] = \begin{bmatrix} \cos(\alpha(t)+\beta_r) & \sin(\alpha(t)+\beta_r) & \left\{ \begin{matrix} \gamma_r \sin(\alpha(t)+ \\ \beta_r - \psi_r) \end{matrix} \right\} \\ -\sin(\alpha(t)+\beta_r) & \cos(\alpha(t)+\beta_r) & \left\{ \begin{matrix} \gamma_r \cos(\alpha(t) \\ +\beta_r - \psi_r) \end{matrix} \right\} \\ \gamma_r \sin\psi_r & -\gamma_r \cos\psi_r & 1 \end{bmatrix} \tag{12}$$

The total position vector locating G_r to the reference point O_r is found by summing equations (7) and (11)

$$\bar{r}_{(OG)_r} = [\epsilon_{r\xi} + \varepsilon_{rG}\cos(\alpha(t)+\beta_r) + d_r\gamma_{r\eta}]\hat{e}_\xi + [\epsilon_{r\eta} + \varepsilon_{rG}\sin(\alpha(t)+\beta_r) - d_r\gamma_{r\xi}]\hat{e}_\eta + [u_{rz} + d_r + \varepsilon_{rG}\gamma_r \sin(\alpha(t)+\beta_r - \psi_r)]\hat{e}_\zeta \tag{13}$$

The absolute acceleration of G_r is evaluated by recognizing that the center of mass G_r translates within a rotating reference frame ($\xi\eta\zeta$), where the angular velocity and acceleration of the frame are provided in Section Inertial Maneuver Profile. Accounting for the acceleration of point O and the rotation of $\xi\eta\zeta$ yields the absolute acceleration of the rotating seal element center of mass

$$\bar{a}_{G_r} = \bar{a}_O + \frac{\partial^2 \bar{r}_{(OG)_r}}{\partial t^2} + \dot{\bar{\lambda}}_0 \times \bar{r}_{(OG)_r} + \bar{\lambda}_0 \times \bar{\lambda}_0 \times \bar{r}_{(OG)_r} + 2\bar{\lambda}_0 \times \frac{\partial \bar{r}_{(OG)_r}}{\partial t} \tag{14}$$

where the partial derivatives signify velocities and accelerations of G_r within the reference frame.

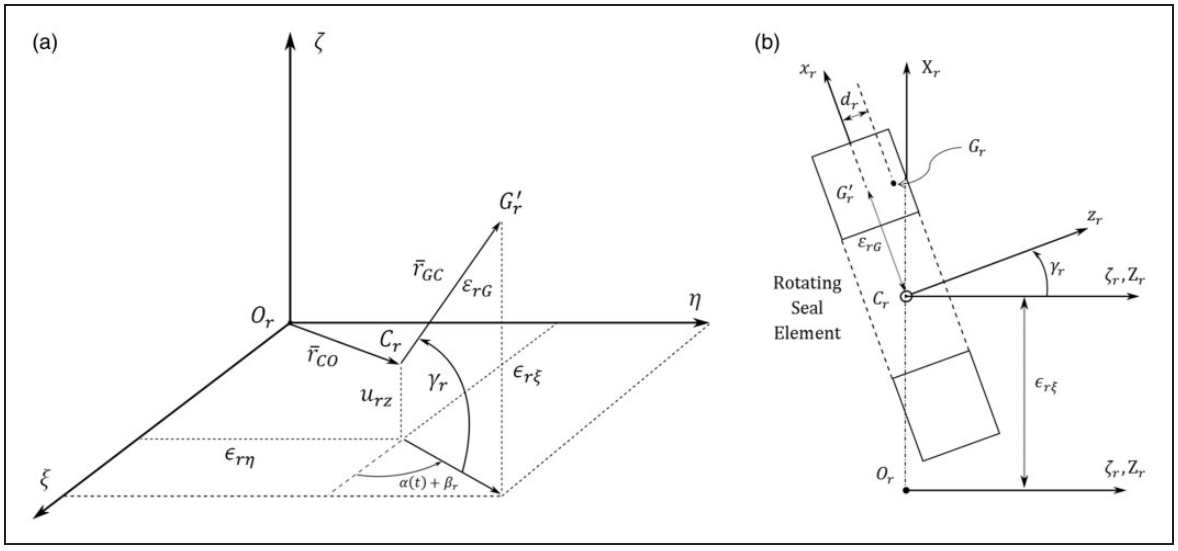

Figure 4. Quantities used to determine the dynamic forces and moments caused by rotating seal element eccentricity. (a) Position analysis of seal seat eccentricities and tilts (d_r not shown for brevity) and (b) imbalance and offset in the rotating seal seat.

Expanding this expression elucidates terms resulting from relative acceleration, maneuver acceleration, centripetal effects, and Coriolis acceleration. Several simplifying assumptions are made for brevity in presenting the expanded results. First, centripetal accelerations resulting from $\bar{\lambda}_0$ are neglected because their overall influence is small compared to centripetal terms resulting from ω_r (i.e. $|\bar{\lambda}_0| < < \omega_r$). Second, any terms resulting in triple products of the imbalance, maneuver rotation components, or the degrees of freedom are neglected since these terms are at most second order. The simplified acceleration is then

$$\begin{aligned}\bar{a}_{G_r} = &[a_{O\xi} + \ddot{\epsilon}_{r\xi} - \varepsilon_{rG}[\omega_r^2\cos(\alpha+\beta_r) + \dot{\omega}_r\sin(\alpha+\beta_r)] \\ &+ d_r\ddot{\gamma}_{r\eta} + 2\lambda_y\dot{u}_{rz} - 2\lambda_{ro}(\dot{\epsilon}_{r\eta} + \varepsilon_{rG}\omega_r\cos(\alpha+\beta_r)) \\ &+ 2\lambda_y\dot{u}_{rz} + \dot{\lambda}_y d_r - \dot{\lambda}_{ro}\varepsilon_{rG}\sin(\alpha+\beta_r)]\hat{e}_\xi \\ &+ [a_{O\eta} + \ddot{\epsilon}_{r\eta} - \varepsilon_{rG}[\omega_r^2\sin(\alpha+\beta_r) - \dot{\omega}_r\cos(\alpha+\beta_r)] \\ &- d_r\ddot{\gamma}_{r\xi} - 2\lambda_p\dot{u}_{rz} + 2\lambda_{ro}(\dot{\epsilon}_{r\xi} - \varepsilon_{rG}\omega_r\sin(\alpha+\beta_r)) \\ &- 2\lambda_p\dot{u}_{rz} - \dot{\lambda}_p d_r + \dot{\lambda}_{ro}\varepsilon_{rG}\cos(\alpha+\beta_r)]\hat{e}_\eta \\ &+ [a_{O\zeta} + \ddot{u}_{rz} + \lambda_p(\dot{\epsilon}_{r\eta} + \varepsilon_{rG}\omega_r\cos(\alpha+\beta_r)) \\ &+ \lambda_y(\varepsilon_{rG}\omega_r\cos(\alpha+\beta_r) - \dot{\epsilon}_{r\eta}) \\ &+ \dot{\lambda}_p\varepsilon_{rG}\sin(\alpha+\beta_r) - \dot{\lambda}_y\varepsilon_{rG}\cos(\alpha+\beta_r)]\hat{e}_\zeta\end{aligned} \tag{15}$$

The acceleration simplifies considerably if inertial maneuver rotations are neglected. Likewise, expanding equation (9) provides the acceleration of the stationary seal element

$$\begin{aligned}\bar{a}_{G_s} = &(a_{O\xi} + \ddot{\epsilon}_{s\xi} - 2\lambda_{ro}\dot{\epsilon}_{s\eta} + 2\lambda_y\dot{u}_{sz})\hat{e}_\xi \\ &+ (a_{O\eta} + \ddot{\epsilon}_{s\eta} + 2\lambda_{ro}\dot{\epsilon}_{s\xi} - 2\lambda_p\dot{u}_{sz})\hat{e}_\eta \\ &+ (a_{O\zeta} + \ddot{u}_{sz} + 2\lambda_p\dot{\epsilon}_{s\eta} - 2\lambda_y\dot{\epsilon}_{s\eta})\hat{e}_\zeta\end{aligned} \tag{16}$$

This work assumes that the stationary element is balanced (i.e. the center of mass aligns identically with C_s), although this restriction could be removed in future works.

Angular kinematics

Non-contacting mechanical face seals can typically only tolerate several milliradians of misalignment before undesirable contact occurs. Consequently, the angular kinematics are simplified by describing the tilt of each element in vector form

$$\bar{\gamma}_s = \gamma_{s\xi}\hat{e}_\xi + \gamma_{s\eta}\hat{e}_\eta \tag{17}$$

$$\bar{\gamma}_r = \gamma_{r\xi}\hat{e}_\xi + \gamma_{r\eta}\hat{e}_\eta \tag{18}$$

The absolute angular velocity of each body has been derived in detail in several other works.[12,14,34,35] For brevity, the results of those works are used here without derivation, and the reader is referred to any of the previous references for further detail. Without including inertial maneuver rotation, the absolute angular velocity of the rotating seal element in the rotating $(xyz)_r$ frame is

$$\bar{\lambda}_r = \dot{\gamma}_r\hat{e}_{x_r} + \dot{\psi}_r\sin\gamma_r\hat{e}_{y_r} + [\dot{\psi}_r(\cos\gamma_r - 1) + \omega_r]\hat{e}_{z_r} \tag{19}$$

The total angular velocity, including inertial maneuver loads, is found by summing equations (5) and (19)

$$\begin{aligned}\bar{\lambda}_r = &(\dot{\gamma}_r + \lambda_p\cos\psi_r + \lambda_y\sin\psi_r)\hat{e}_{x_r} \\ &+ (\dot{\psi}_r\sin\gamma_r + \gamma_r\lambda_{ro} + \lambda_y\cos\psi_r - \lambda_p\sin\psi_r)\hat{e}_{y_r} \\ &+ [\dot{\psi}_r(\cos\gamma_r - 1) + \omega_r + \lambda_{ro} - \gamma_r\lambda_y\cos\psi_r \\ &+ \lambda_p\sin\psi_r]\hat{e}_{z_r}\end{aligned} \tag{20}$$

The dynamic moments will depend on the time rate-of-change of $\bar{\lambda}_r$ within the $x_r y_r z_r$ frame

$$\begin{aligned}\frac{\partial\bar{\lambda}_r}{\partial t} = &[\ddot{\gamma}_r + \dot{\lambda}_p\cos\psi_r - \lambda_p\dot{\psi}_r\sin\psi_r \\ &+ \dot{\lambda}_y\sin\psi_r + \lambda_y\dot{\psi}_r\cos\psi_r]\hat{e}_{x_r} \\ &+ [\ddot{\psi}_r\sin\gamma_r + \dot{\psi}_r\dot{\gamma}_r\cos\gamma_r + \dot{\gamma}_r\lambda_{ro} + \gamma_r\dot{\lambda}_{ro} \\ &+ \dot{\lambda}_y\cos\psi_r - \lambda_y\dot{\psi}_r\sin\psi_r \\ &- \dot{\lambda}_p\sin\psi_r - \lambda_p\dot{\psi}_r\cos\psi_r]\hat{e}_{y_r} \\ &+ [\ddot{\psi}_r(\cos\gamma_r - 1) - \dot{\psi}_r\dot{\gamma}_r\sin\gamma_r + \dot{\omega}_r + \dot{\lambda}_{ro} \\ &- \dot{\gamma}_r\lambda_y\cos\psi_r - \gamma_r\dot{\lambda}_y\cos\psi_r + \gamma_r\lambda_y\dot{\psi}_r\sin\psi_r \\ &+ \dot{\lambda}_p\sin\psi_r + \lambda_p\dot{\psi}_r\cos\psi_r]\hat{e}_{z_r}\end{aligned} \tag{21}$$

Surface velocities of seal element

Fluid pressures exist at every point p within the sealing dam, and contact pressures are generated if the relative clearance and surface roughness dimension are comparable in magnitude. The locations on the seal elements commensurate with point p in the sealing dam are denoted p_s and p_r for the stationary and rotating seal elements. The position and velocity of these points must be found to determine the fluid and contact pressures. For consistent comparison, these quantities must be described using the same coordinate system. The maneuver velocities act with parity on both seal elements, and therefore, do not affect the fluid pressure or shear forces. Furthermore, this work assumes that the rotating element is always contained entirely within the bounds of the stationary element (see Figure 3(a)).

The geometry of the sealing apparatus lends itself naturally to a polar coordinate description; here, a polar coordinate system (r, θ) will be referenced relative to the rotating seal element's center. The unit vectors defining the $\xi\eta$ and $r\theta$ frames are related by the

following rotation transformation

$$\begin{Bmatrix} \hat{e}_\xi \\ \hat{e}_\eta \\ \hat{e}_\zeta \end{Bmatrix} = \begin{bmatrix} \cos\theta & -\sin\theta & 0 \\ \sin\theta & \cos\theta & 0 \\ 0 & 0 & 1 \end{bmatrix} \begin{Bmatrix} \hat{e}_r \\ \hat{e}_\theta \\ \hat{e}_\zeta \end{Bmatrix} \tag{22}$$

The points p_r and p_s are located relative to the rotating and stationary seal element geometric centers by the vectors $\bar{r}_1$ and $\bar{r}_2$, respectively, as shown in Figure 3(a). In the polar coordinate frame, these vectors are

$$\bar{r}_1 = r\hat{e}_r \tag{23}$$

$$\begin{aligned} \bar{r}_2 &= \bar{r}_1 - \bar{\epsilon}^* \\ &= [r + (\epsilon_{r\xi} - \epsilon_{s\xi})\cos\theta + (\epsilon_{r\eta} - \epsilon_{s\eta})\sin\theta]\hat{e}_r \\ &\quad + [(\epsilon_{r\eta} - \epsilon_{s\eta})\cos\theta - (\epsilon_{r\xi} - \epsilon_{s\xi})\sin\theta]\hat{e}_\theta \end{aligned} \tag{24}$$

Every point p_s on the stationary element has the same velocity in the $\xi\eta$ frame because the element does not rotate about ζ. The velocity $\bar{V}_{ps}$ is then always equal to the velocity of point C_s

$$\begin{aligned} \bar{V}_{ps} &= \dot{\epsilon}_{s\xi}\hat{e}_\xi + \dot{\epsilon}_{s\eta}\hat{e}_\eta = (\dot{\epsilon}_{s\xi}\cos\theta + \dot{\epsilon}_{s\eta}\sin\theta)\hat{e}_r \\ &\quad + (\dot{\epsilon}_{s\eta}\cos\theta - \dot{\epsilon}_{s\xi}\sin\theta)\hat{e}_\theta \end{aligned} \tag{25}$$

The velocity of every point p_r on the rotating element accrues an additional contribution from the element's rotation ω_r

$$\begin{aligned} \bar{V}_{pr} &= \dot{\epsilon}_{r\xi}\hat{e}_\xi + \dot{\epsilon}_{r\eta}\hat{e}_\eta + \bar{\omega}_r \times \bar{r}_1 \\ &= (\dot{\epsilon}_{r\xi}\cos\theta + \dot{\epsilon}_{r\eta}\sin\theta)\hat{e}_r \\ &\quad + (r\omega_r + \dot{\epsilon}_{r\eta}\cos\theta - \dot{\epsilon}_{r\xi}\sin\theta)\hat{e}_\theta \end{aligned} \tag{26}$$

The fluid pressure depends on the relative radial and tangential velocities between points p_s and p_r.[16,19] To avoid a confusion in nomenclature, the fluid pressure equations label the rotating and stationary seal elements as elements 1 and 2, respectively. Using this notation, the component velocities are

$$V_{1r} = \dot{\epsilon}_{r\xi}\cos\theta + \dot{\epsilon}_{r\eta}\sin\theta \tag{27}$$

$$V_{2r} = \dot{\epsilon}_{s\xi}\cos\theta + \dot{\epsilon}_{s\eta}\sin\theta \tag{28}$$

$$V_{1\theta} = r\omega_r + \dot{\epsilon}_{r\eta}\cos\theta - \dot{\epsilon}_{r\xi}\sin\theta \tag{29}$$

$$V_{2\theta} = \dot{\epsilon}_{s\eta}\cos\theta - \dot{\epsilon}_{s\xi}\sin\theta \tag{30}$$

Applied fluid and contact forces

The seal element dynamics are inextricably coupled by fluid and contact forces that exist within the sealing dam. These forces depend on the complex interactions between fluid pressures, fluid shear, surface roughness, and friction, all of which are influenced strongly by the system dynamics (as described using the kinematic expressions provided in earlier sections). The requisite relationship required for deriving the fluid and contact forces is the clearance between the seal elements (i.e. the fluid film thickness), which is discussed first. The fluid and contact forces are then derived as a function of the clearance.

Film thickness

The fluid film clearance, shown in Figure 3(b), is the axial offset between corresponding points on the stationary and rotating seal elements, and contains contributions from axial and angular deflections in addition to the seal face geometry contributions. To ensure consistency, the film thickness $h(r,\theta)$ is given with respect to the polar coordinate system attached to the rotating seal element center

$$\begin{aligned} h(r,\theta) &= C_o + (u_{sz} - u_{rz}) + (\bar{\gamma}_s \times \bar{r}_2 - \bar{\gamma}_r \times \bar{r}_1) \\ &\quad \cdot \hat{e}_\zeta + \beta(t)(r - r_i) \end{aligned} \tag{31}$$

where the coning $\beta(t)$ is left as a general function of time since it depends on transient thermoelastic deformations of the seal faces. Using each element's constitutive tilt components is judicious because it simplifies derivatives of the film thickness and allows any function of the film thickness to be written in terms of the degrees-of-freedom. Thus, the clearance and its derivatives can be evaluated directly during the numeric integration solution process without any additional calculations. Evaluating equation (31) indicates that film thickness variations caused by relative eccentricity are of order $O(\gamma\epsilon)$ (see Wileman and Green[19] for a more detailed depiction of these effects). Neglecting these second-order effects gives the total film thickness

$$\begin{aligned} h(r,\theta) &= C_o + (u_{sz} - u_{rz}) + (\gamma_{s\xi} - \gamma_{r\xi})r\sin\theta \\ &\quad - (\gamma_{s\eta} - \gamma_{r\eta})r\cos\theta + \beta(t)(r - r_i) \end{aligned} \tag{32}$$

Spatial and temporal derivatives of equation (32) will be useful for calculating the fluid pressure

$$\frac{\partial h}{\partial r} = (\gamma_{s\xi} - \gamma_{r\xi})\sin\theta - (\gamma_{s\eta} - \gamma_{r\eta})\cos\theta + \beta(t) \tag{33}$$

$$\frac{\partial h}{\partial \theta} = (\gamma_{s\xi} - \gamma_{r\xi})r\cos\theta + (\gamma_{s\eta} - \gamma_{r\eta})r\sin\theta \tag{34}$$

$$\begin{aligned} \frac{\partial h}{\partial t} &= \dot{u}_{sz} - \dot{u}_{rz} + (\dot{\gamma}_{s\xi} - \dot{\gamma}_{r\xi})r\sin\theta \\ &\quad - (\dot{\gamma}_{s\eta} - \dot{\gamma}_{r\eta})r\cos\theta + \dot{\beta}(t)(r - r_i) \end{aligned} \tag{35}$$

Fluid and contact axial pressure

The fluid film couples the rotating and stationary seal elements, allowing one element to track misalignments

in the other. The fluid pressure in the sealing dam is found by solving the Reynolds equation for a narrow seal, which has previously been performed for an FMSR-E seal by Wileman and Green.[19] The resulting fluid pressure profile contains contributions from static[5] and hydrodynamic effects

$$P_s(r,\theta) = P_o - (P_o - P_i)\frac{h_i^2}{h_o^2 - h_i^2}\left[\left(\frac{h_o}{h}\right)^2 - 1\right] \quad (36)$$

$$\begin{aligned} P_d(r,\theta) = -3\mu\frac{(r_o - r)(r - r_i)}{h_m h^2}\Bigg[2\frac{\partial h}{\partial t} + (V_{1r} - V_{2r})\frac{\partial h}{\partial r} \\ + \frac{(V_{1\theta} - V_{2\theta})}{r}\frac{\partial h}{\partial \theta} + h\frac{\partial}{\partial r}(V_{1r} + V_{2r}) \\ + \frac{h}{r}\frac{\partial}{\partial \theta}(V_{1\theta} + V_{2\theta}) + \frac{h}{r}(V_{1r} + V_{2r})\Bigg] \end{aligned} \quad (37)$$

where μ is the fluid viscosity and h_i, h_o, and h_m are the values of the film thickness at the inner, outer, and mean radii of the smaller element, which in this case is the rotating seal element. The relative velocity components and film thickness kinematics are given in equations (27) to (30) and equations (32) to (35), respectively.

Contact occurs between the seal faces when the relative film thickness at any point in the sealing dam approaches the same order of magnitude as the surface roughness. The contact pressure $P_c(r,\theta)$ as a function of film thickness has previously been derived using the elasto-plastic Jackson-Green rough surface contact model.[24,36,37] Approximating the pressure–film thickness relationship using an exponential expression significantly improves computation speed when the system dynamics are simulated[37]

$$P_c(r,\theta) = C_1 \exp(C_2 h(r,\theta)) \quad (38)$$

where C_1 and C_2 depend on the surface asperity geometry and material properties. Employing a rough surface contact model to approximate the contact pressure is advantageous because the contact pressure depends on real and measurable surface properties rather than implicit assumptions regarding the force–displacement relationship. In addition, an elasto-plastic model is required because one seal surface is typically much harder than the other.[26]

The total pressure $P(r,\theta)$ acting at any point in the sealing dam is the sum of the contributions from static fluid pressure (equation (36)), dynamic fluid pressure (equation (37)), and contact pressure (equation (38)). The moments caused by fluid and contact pressure acting on the seal faces are not equal and opposite because of eccentric deflections of both elements (i.e. the moments are evaluated about different points, C_r and C_s). Furthermore, care must be taken when deriving the contact moment acting on the stationary element because the contact and fluid pressures are defined relative to a polar frame fixed to the rotating element. In vector form, the forces and moments caused by normal fluid and contact pressure are

$$\bar{F}_{s\zeta} = \int_{r_i}^{r_o}\int_0^{2\pi} P(r,\theta) r \mathrm{d}r\mathrm{d}\theta \quad (39)$$

$$\bar{M}_r = \int_{r_i}^{r_o}\int_0^{2\pi} -[\bar{r}_1 \times P(r,\theta)\hat{e}_\zeta] r \mathrm{d}r\mathrm{d}\theta \quad (40)$$

$$\bar{M}_s = \int_{r_i}^{r_o}\int_0^{2\pi} [\bar{r}_2 \times P(r,\theta)\hat{e}_\zeta] r \mathrm{d}r\mathrm{d}\theta \quad (41)$$

In these expressions, the integral bounds are dictated by the element with smaller radii, which in this work is the rotating element. The net axial force acting on the rotating and stationary elements is equal and opposite, i.e. $\bar{F}_{r\zeta} = -\bar{F}_{s\zeta}$. Since these forces are equal and opposite, the element subscript is dropped ($\bar{F}_{s\zeta} = \bar{F}_\zeta$ and $F_{r\zeta} = -F_\zeta$) while retaining the correct sign in the equation of motion. The moments acting on the rotating element from axial fluid and contact pressures do not depend on the relative eccentricity because the polar coordinate system $r\theta$ is defined relative to the element's center, O_r. The moments acting about the stationary element's center, however, are more complex since they act about a point that is not the center of the $r\theta$ system. Equations (39) to (41) are expanded into component form in Appendix 1.

Friction forces

Friction forces are generated by relative tangential motion between the surfaces at the contact locations, and therefore these forces incur contributions from both relative translation and relative rotation. A dry Coulomb friction law with coefficient μ_f is used here to relate the contact pressure $P_c(r,\theta)$ to the shear stress at each point in the sealing dam. The friction shear stress acts to oppose relative velocity between the surfaces and varies depending on position $r\theta$ (for the rotating seal element, this direction is labeled $\hat{e}_{fr}(r,\theta)$). The direction is calculated using the relative velocity between corresponding points on the rotating and stationary seal elements

$$\hat{e}_{fr}(r,\theta) = -\frac{\bar{V}_{pr} - \bar{V}_{ps}}{\|\bar{V}_{pr} - \bar{V}_{ps}\|} \quad (42)$$

The shear stress direction on the stationary seal element is opposite to that given in equation (42). The relative velocity in the $\xi\eta\zeta$ frame is

$$\bar{V}_{pr} - \bar{V}_{ps} = (-\dot{\epsilon}_\xi^* - r\omega_r \sin\theta)\hat{e}_\xi + (-\dot{\epsilon}_\eta^* + r\omega_r \cos\theta)\hat{e}_\eta \quad (43)$$

and its magnitude, after eliminating second order terms, is

$$\left\| \bar{V}_{pr} - \bar{V}_{ps} \right\|^2 = r\omega_r(r\omega_r + 2\dot{\epsilon}^*_\xi \sin\theta - 2\dot{\epsilon}^*_\eta \cos\theta) \approx r^2\omega_r^2 \tag{44}$$

Mathematically, the above approximation is reasonable since $r\omega_r >> \dot{\epsilon}^*_{\xi,\eta}$, while intuitively, the approximation implies that the circumferential velocity caused by shaft rotation is much greater than the relative translational velocity. In this manner, the friction shear stress acting on seal element j is

$$\bar{\tau}_{fj}(r,\theta) = \mu_f P_{cj}(r,\theta)\hat{e}_{fj}(r,\theta) \tag{45}$$

The total friction force acting on seal element j is obtained by integrating equation (45) across the sealing dam

$$\bar{F}_{fj} = \int_{r_i}^{r_o}\int_0^{2\pi} \mu_f P_{cj}(r,\theta)\hat{e}_{fj}(r,\theta) r \mathrm{d}r\mathrm{d}\theta \tag{46}$$

The contact shear stress also generates a net moment about each element's center because of the element's tilt. In vector form, the moments acting on the stationary and rotating seal elements are

$$\bar{M}_{fs} = \int_{r_i}^{r_o}\int_0^{2\pi} -[(\bar{r}_2 + \bar{\gamma}_s \times \bar{r}_2) \times \mu_f P_c(r,\theta)\hat{e}_{fr}(r,\theta)] r \mathrm{d}r\mathrm{d}\theta \tag{47}$$

$$\bar{M}_{fr} = \int_{r_i}^{r_o}\int_0^{2\pi} [(\bar{r}_1 + \bar{\gamma}_r \times \bar{r}_1) \times \mu_f P_c(r,\theta)\hat{e}_{fr}(r,\theta)] r \mathrm{d}r\mathrm{d}\theta \tag{48}$$

Component forms of these vector expressions are provided in Appendix 1.

Fluid shear forces and moments

Relative motion between the seal faces induces fluid shear stresses, which are calculated by assuming Couette flow (Etsion and Sharoni[21] demonstrate that the pressure-driven Poiseuille component is negligible in narrow eccentric face seals). The Couette shear stresses $\bar{\tau}_{\mu j}$ acting on body j only depend on the fluid velocities $\bar{v}$ between body j and body i

$$\bar{\tau}_{\mu j}(r,\theta) = \mu \frac{\partial \bar{v}}{\partial \zeta} \tag{49}$$

where $\bar{v}$ denotes the velocity of the fluid between the seal faces. This derivative is approximated by dividing the relative velocity between bodies j and i, $\bar{V}_{pj} - \bar{V}_{pi}$ by the film thickness $h(r,\theta)$. The relative velocity between corresponding points on the seal elements is given in equation (43). Integrating equation (49) over the sealing dam provides the fluid shear forces

$$\begin{aligned}\bar{F}_{\mu r}(r,\theta) = \mu \int_{r_i}^{r_o}\int_0^{2\pi} [&\frac{-\dot{\epsilon}^*_\xi - r\omega_r \sin\theta}{h(r,\theta)}\hat{e}_\xi \\ &+ \frac{-\dot{\epsilon}^*_\eta + r\omega_r \cos\theta}{h(r,\theta)}\hat{e}_\eta] r \mathrm{d}r\mathrm{d}\theta\end{aligned} \tag{50}$$

$$\bar{F}_{\mu s}(r,\theta) = -\bar{F}_{\mu r}(r,\theta) \tag{51}$$

where the fluid shear force acting on the stationary seal element is obtained by recognizing that an observer fixed to the element sees a relative velocity with opposite sign. The fluid shear stresses also generate moments about each element's geometric center because of relative tilt and eccentricity. These moments are

$$\bar{M}_{\mu s} = \int_{r_i}^{r_o}\int_0^{2\pi} -[(\bar{r}_2 + \bar{\gamma}_s \times \bar{r}_2) \times \bar{\tau}_{\mu r}(r,\theta)] r \mathrm{d}r\mathrm{d}\theta \tag{52}$$

$$\bar{M}_{\mu r} = \int_{r_i}^{r_o}\int_0^{2\pi} [(\bar{r}_1 + \bar{\gamma}_r \times \bar{r}_1) \times \bar{\tau}_{\mu r}(r,\theta)] r \mathrm{d}r\mathrm{d}\theta \tag{53}$$

Importantly, the effects from eccentricity in the fluid shear moments are second-order and are therefore eliminated from the analysis. The components of equations (53) and (52) are given in Appendix 1.

Support forces: Coupled rotordynamics

The rotating seal element is flexibly attached to the rotor, which also experiences angular, lateral, and/or axial deflections. The effects of coupled rotordynamics have historically been neglected in the analysis of mechanical face seals. Here, the 'rotor' consists of the flexible shaft and attached rigid disk on which the rotating seal element is affixed (see Figure 1).

The rotating element degrees-of-freedom were judiciously chosen to be absolute in the system-fixed $\xi\eta\zeta$ reference frame to reduce the mathematical and intuitive overhead associated with coupling between the rotor and rotating seal element. Because the degrees-of-freedom are absolute, the coupling between the rotor and the rotating seal element only manifests in the forces induced by support stiffness and damping. These forces depend on the relative deflections between the seal and rotor, where the rotor degrees of freedom are denoted with subscript 'R'. The support force is

$$\begin{aligned}\bar{F}_{s\epsilon,r} = &[-K_{r\epsilon}(\epsilon_{r\xi} - \epsilon_{R\xi}) - D_{r\epsilon}(\dot{\epsilon}_{r\xi} - \dot{\epsilon}_{R\xi})]\hat{e}_\xi \\ &+ [-K_{r\epsilon}(\epsilon_{r\eta} - \epsilon_{R\eta}) - D_{r\epsilon}(\dot{\epsilon}_{r\eta} - \dot{\epsilon}_{R\eta})]\hat{e}_\eta \\ &+ [-K_{rz}(u_{rz} - u_{Rz}) - D_{rz}(\dot{u}_{rz} - \dot{u}_{Rz})]\hat{e}_\zeta\end{aligned} \tag{54}$$

where the eccentric stiffness and damping coefficients are $K_{r\epsilon}$ and $D_{r\epsilon}$, and the axial stiffness and damping

coefficients are K_{rz} and D_{rz}. Finally, the support moment is

$$\begin{aligned}\bar{M}_{sr} = &[-K_r(\gamma_{r\xi} - \gamma_{R\xi}) - D_r(\dot{\gamma}_{r\xi} - \dot{\gamma}_{R\xi}) - \omega_r D_r(\gamma_{r\eta} - \gamma_{R\eta})]\hat{e}_\xi \\ &+ [-K_r(\gamma_{r\eta} - \gamma_{R\eta}) - D_r(\dot{\gamma}_{r\eta} - \dot{\gamma}_{R\eta}) + \omega_r D_r(\gamma_{r\xi} - \gamma_{R\xi})]\hat{e}_\eta\end{aligned} \tag{55}$$

Equation (55) includes the effect of rotating damping caused by the flexible seal support. In low-temperature applications, the rotating seal element is often supported using an axial spring and a circumferential viscoelastic O-ring. Because the O-ring is viscoelastic, the stiffness and damping properties are a function of excitation frequency. However, the stiffness and damping of the fluid film in a liquid-lubricated seal is typically several orders of magnitude greater than the support stiffness and damping.[35] For liquid-lubricated seals such as those considered here, this disparity makes it reasonable to neglect variations in the support properties caused by changes in the excitation frequency.

Dynamic moments of the rotating seal element

The dynamic moments acting on the rotating seal element depend on its angular momentum. To remain consistent with earlier works, the angular momentum is derived relative to the geometric center C_r

$$\bar{h}_{C_r} = [I_{C_r}]\bar{\lambda}_r \tag{56}$$

The angular momentum will first be expressed using the rotating (i.e. nutating) $x_r y_r z_r$ reference frame, and then transformed back into the $\xi\eta\zeta$ system-fixed frame prior to evaluating the dynamic moments (i.e. the time rate of change of the angular momentum).

Geometry, installation errors, and/or manufacturing imperfections may cause the principal axes $x_r^p y_r^p z_r^p$ to be misaligned from the spin axes $1_r 2_r 3_r$. This effect is referred to here as dynamic angular misalignment. The misalignment magnitude is χ and is assumed to occur about the principal 1_r axis without loss of generality. As discussed in Section Reference Frames, the kinematic constraint between the precession and spin[14,34] is $\phi = \alpha(t) - \psi_r$, and will be useful for deriving the dynamic misalignment moments. For small misalignments $\chi << 1$, the rotation transformation between the principal axes and the nutating axes $(x_r y_r z_r)$ is

$$[R] = \begin{bmatrix} \cos\phi & \sin\phi & 0 \\ -\sin\phi & \cos\chi & \chi \\ \chi\sin\phi & -\chi\cos\phi & 1 \end{bmatrix} \tag{57}$$

The principal inertia tensor $[I_{C_r}]$ is transformed into the nutating reference frame $x_r y_r z_r$

$$\begin{aligned}[I_{C_r}]^{x_r y_r x_r} &= [R]^T \begin{bmatrix} I_{tr} & 0 & 0 \\ 0 & I_{tr} & 0 \\ 0 & 0 & I_{pr} \end{bmatrix}^{x_r^p y_r^p z_r^p} \\ [R] &= \begin{bmatrix} I_{tr} + (I_{pr} - I_{tr})\chi^2 \sin^2\phi & -\frac{1}{2}\chi^2(I_{pr} - I_{tr})\sin 2\phi & (I_{pr} - I_{tr})\chi\sin\phi \\ -\frac{1}{2}\chi^2(I_{pr} - I_{tr})\sin 2\phi & I_{tr} & -(I_{pr} - I_{tr})\chi\cos\phi \\ (I_{pr} - I_{tr})\chi\sin\phi & -(I_{pr} - I_{tr})\chi\cos\phi & I_{pr} \end{bmatrix}\end{aligned} \tag{58}$$

using equation (57)

For small misalignments, this result reduces to the following

$$[I_{C_r}] = \begin{bmatrix} I_{tr} & 0 & \begin{Bmatrix} (I_{pr} - I_{tr}) \\ \chi\sin\phi \end{Bmatrix} \\ 0 & I_{tr} & \begin{Bmatrix} -(I_{pr} - I_{tr}) \\ \chi\cos\phi \end{Bmatrix} \\ \begin{Bmatrix} (I_{pr} - I_{tr}) \\ \chi\sin\phi \end{Bmatrix} & \begin{Bmatrix} -(I_{pr} - I_{tr}) \\ \chi\cos\phi \end{Bmatrix} & I_{pr} \end{bmatrix} \tag{59}$$

Recognizing that C_r is an accelerating reference point that is not the center of mass, the dynamic moment acting on the rotating seal element is

$$\Sigma\bar{M}_{dyn} = \frac{\partial\bar{h}_{C_r}}{\partial t} + \bar{\omega}_{(xyz)_r} \times \bar{h}_{C_r} + \bar{r}_{(GC)_r} \times m_r\bar{a}_{C_r} \tag{60}$$

where

$$\frac{\partial\bar{h}_{C_r}}{\partial t} = [I_{C_r}]\dot{\bar{\lambda}}_r + \frac{\partial([I_{C_r}])}{\partial t}\bar{\lambda}_r \tag{61}$$

The angular velocity of the $x_r y_r z_r$ reference frame is denoted $\bar{\omega}_{(xyz)_r}$

$$\bar{\omega}_{(xyz)_r} = \dot{\gamma}_r\hat{e}_{x_r} + \dot{\psi}_r\sin\gamma_r\hat{e}_{y_r} + \dot{\psi}_r\cos\gamma_r\hat{e}_{z_r} + \bar{\lambda}_0 \tag{62}$$

In reality, the inertial maneuver rotations are likely to be much smaller than the shaft rotation rate ω_r. Hence, the products of the orthogonal inertial rotations are much smaller than the products of any inertial rotation with the shaft speed.

The dynamic moments must now be transformed from the nutating reference frame $x_r y_r z_r$ into the system-fixed reference frame $\xi\eta\zeta$ to maintain consistency with the applied forces derived earlier in the chapter. This task is accomplished using the following rotation transformation, where the subscript indicates the axis about which the rotation occurs and the term in parenthesis indicates the magnitude of the rotation

$$(\bar{M}_{dyn})_{\xi\eta\zeta} = [R_{Z_r}(\psi_r)]^T[R_{x_r}(\gamma_r)]^T\left(\frac{\partial \bar{h}_{C_r}}{\partial t} + \bar{\omega}_{(xyz)_r} \times \bar{h}_{C_r}\right) + \bar{r}_{(GC)_r} \times m_r \bar{a}_{C_r} \tag{63}$$

It is important to note that the term $\bar{r}_{(GC)_r} \times m_r \bar{a}_{C_r}$ has already been provided in the system-fixed reference frame $\xi\eta\zeta$. Finally, the inertial degrees-of-freedom are instituted in the equations of motion using the following relationships

$$\gamma_{r\xi} = \gamma_r \cos\psi_r \tag{64}$$

$$\dot{\gamma}_{r\xi} = \dot{\gamma}_r \cos\psi_r - \gamma_r \dot{\psi}_r \sin\psi_r \tag{65}$$

$$\ddot{\gamma}_{r\xi} = \ddot{\gamma}_r \cos\psi_r - 2\dot{\gamma}_r\dot{\psi}_r \sin\psi_r - \gamma_r\ddot{\psi}_r \sin\psi_r - \gamma_r\dot{\psi}_r^2 \cos\psi_r \tag{66}$$

and

$$\gamma_{r\eta} = \gamma_r \sin\psi_r \tag{67}$$

$$\dot{\gamma}_{r\eta} = \dot{\gamma}_r \sin\psi_r + \gamma_r\dot{\psi}_r \cos\psi_r \tag{68}$$

$$\ddot{\gamma}_{r\eta} = \ddot{\gamma}_r \sin\psi_r + 2\dot{\gamma}_r\dot{\psi}_r \cos\psi_r + \gamma_r\ddot{\psi}_r \cos\psi_r - \gamma_r\dot{\psi}_r^2 \sin\psi_r \tag{69}$$

Evaluating equation (63) is tedious and leads to a number of terms involving the rotating seal element degrees-of-freedom and the maneuver rotation rates λ_p, λ_y, and λ_{ro}. In this work, the influence of $\bar{\lambda}_0$ is retained only in terms involving products of either three maneuver rotation rates with the shaft rotation rate. The intermediate operations leading to the dynamic moments amount to algebraic substitutions, and are therefore omitted here for brevity.

Equations of motion

The equations of motion governing angular deflections of the rotating seal element, including inertial maneuver loads and coupled rotordynamics, are

$$\Sigma\bar{M}_{C_r}: \quad [R_{Z_r}(\psi_r)]^T[R_{x_r}(\gamma_r)]^T\left(\frac{\partial \bar{h}_{C_r}}{\partial t} + \bar{\omega}_{(xyz)_r} \times \bar{h}_{C_r}\right) + \bar{r}_{(GC)_r} \times m_r\bar{a}_{C_r} = +\bar{r}_{(GC)_r} \times \bar{F}_{gr} + \bar{M}_{sr} + \bar{M}_{fr} + \bar{M}_{\mu r} + \bar{M}_r + \bar{M}_{ri} \tag{70}$$

$$\Sigma\bar{F}_{G_r}: \quad m_r\bar{a}_{G_r} = \bar{F}_{gr} + \bar{F}_{zr} + \bar{F}_{\mu r} + \bar{F}_{fr} + \bar{F}_{sr} + \bar{F}_{ri} \tag{71}$$

where the applied forces and moments arise from static misalignment ($\bar{M}_{ri}$ and $\bar{F}_{ri}$), gravity $\bar{F}_{gr}$, the flexible supports ($\bar{M}_{sr}$ and $\bar{F}_{sr}$), fluid shear ($\bar{M}_{\mu r}$ and $\bar{F}_{\mu r}$), friction ($\bar{M}_{fr}$ and $\bar{F}_{fr}$), and normal fluid and contact pressure ($\bar{M}_r$ and $\bar{F}_\zeta$). Expanding these equations in component form gives

$$\begin{aligned} &I_{tr}\ddot{\gamma}_{r\xi} + I_{pr}(\omega_r\dot{\gamma}_{r\eta} + \dot{\omega}_r\gamma_{r\eta}) + D_r(\dot{\gamma}_{r\xi} - \dot{\gamma}_{R\xi}) + K_r(\gamma_{r\xi} - \gamma_{R\xi}) \\ &\quad + \omega_r D_r(\gamma_{r\eta} - \gamma_{R\eta}) = m_r g d_r + (M_{fr})_\xi + (M_{\mu r})_\xi \\ &\quad + M_{r\xi} + K_r\chi_s\cos(\alpha + \beta_{\chi r}) + (I_{tr} - I_{pr}) \\ &\quad \chi(\omega_r^2\cos\alpha + \dot{\omega}_r\sin\alpha) - I_{tr}(\dot{\lambda}_p - \lambda_y\dot{\psi}_r) - I_{pr}\lambda_y\omega_r \\ &\quad - m_r\{a_{O\zeta}[\varepsilon_{rG}\sin(\alpha + \beta_r) - d_r\gamma_{r\xi}] - d_r(a_{O\eta} + \ddot{\epsilon}_{r\eta})\} \end{aligned} \tag{72}$$

$$\begin{aligned} &I_{tr}\ddot{\gamma}_{r\eta} - I_{pr}(\omega_r\dot{\gamma}_{r\xi} + \dot{\omega}_r\gamma_{r\xi}) + D_r(\dot{\gamma}_{r\eta} - \dot{\gamma}_{R\eta}) \\ &\quad + K_r(\gamma_{r\eta} - \gamma_{R\eta}) - \omega_r D_r(\gamma_{r\xi} - \gamma_{R\xi}) = \\ &\quad (M_{fr})_\eta + (M_{\mu r})_\eta + M_{r\eta} + K_r\chi_s\sin(\alpha + \beta_{\chi r}) \\ &\quad + (I_{tr} - I_{pr})\ \chi(\omega_r^2\sin\alpha - \dot{\omega}_r\cos\alpha) \\ &\quad - I_{tr}(\dot{\lambda}_y + \lambda_p\dot{\psi}_r) + I_{pr}\lambda_p\omega_r \\ &\quad + m_r\{a_{O\zeta}[\varepsilon_{rG}\cos(\alpha + \beta_r) + d_r\gamma_{r\eta}] - d_r(a_{O\xi} + \ddot{\epsilon}_{r\xi})\} \end{aligned} \tag{73}$$

The static misalignment χ_s is caused by unavoidable imperfections such as improper installation, rotor bow, run-out, etc., and persists even when $\omega_r = 0$. This misalignment is imposed by applying a moment to the rotating seal element that generates χ_s[11]; the line about which χ_s occurs is referenced from axis X_r by the phase angle $\beta_{\chi r}$ (or, alternatively, referenced from ξ_r by the angle $\beta_{\chi r} + \alpha$). The equation of motion governing axial deflections is

$$\begin{aligned} &m_r\ddot{u}_{rz} + D_{rz}(\dot{u}_{rz} - \dot{u}_{Rz}) + K_{rz}(u_{rz} - u_{Rz}) = -F_\zeta + F_{cls} \\ &\quad - m_r[a_{O\zeta} + \dot{\lambda}_p\varepsilon_{rG}\sin(\alpha + \beta_r) \\ &\quad - \dot{\lambda}_y\varepsilon_{rG}\cos(\alpha + \beta_r) + 2\lambda_p(\dot{\epsilon}_{r\eta} + \varepsilon_{rG}\omega_r\cos(\alpha + \beta_r)) \\ &\quad + 2\lambda_y(\varepsilon_{rG}\omega_r\cos(\alpha + \beta_r) - \dot{\epsilon}_{r\xi})] \end{aligned} \tag{74}$$

while those for eccentric deflections are

$$\begin{aligned} &m_r\ddot{\epsilon}_{r\xi} + D_{r\epsilon}(\dot{\epsilon}_{r\xi} - \dot{\epsilon}_{R\xi}) + K_{r\epsilon}(\epsilon_{r\xi} - \epsilon_{R\xi}) = (F_{fr})_\xi \\ &\quad + (F_{\mu r})_\xi - m_r(a_{O\xi} - d_r\ddot{\gamma}_{r\eta}) \\ &\quad + m_r\varepsilon_{rG}[\omega_r^2\cos(\alpha + \beta_r) + \dot{\omega}_r\sin(\alpha + \beta_r)] \\ &\quad + m_r[2\lambda_{ro}(\dot{\epsilon}_{r\eta} + \varepsilon_{rG}\omega_r\cos(\alpha + \beta_r)) \\ &\quad - 2\lambda_y\dot{u}_{rz} - \dot{\lambda}_y d_r + \dot{\lambda}_{ro}\varepsilon_{rG}\sin(\alpha + \beta_r)] \end{aligned} \tag{75}$$

$$m_r\ddot{\epsilon}_{r\eta} + D_{r\epsilon}(\dot{\epsilon}_{r\eta} - \dot{\epsilon}_{R\eta}) + K_{r\epsilon}(\epsilon_{r\eta} - \epsilon_{R\eta}) = (F_{fr})_\eta + (F_{\mu r})_\eta - m_r(a_{O\eta} + g + d_r\ddot{\gamma}_{r\xi}) + m_r\varepsilon_{rG}[\omega_r^2\sin(\alpha+\beta_r) - \dot{\omega}_r\cos(\alpha+\beta_r)] - m_r[2\lambda_{ro}(\dot{\epsilon}_{r\xi} - \varepsilon_{rG}\omega_r\sin(\alpha+\beta_r)) - 2\lambda_p\dot{u}_{rz} - \dot{\lambda}_p d_r + \dot{\lambda}_{ro}\varepsilon_{rG}\cos(\alpha+\beta_r)] \tag{76}$$

where the closing force on the seal is

$$F_{cls} = F_{spr} + \pi\left[P_o(r_o^2 - r_b^2) + P_i(r_b^2 - r_i^2)\right] \tag{77}$$

The supporting secondary spring force is F_{spr}, while the radii in the above equation pertain to the rotating seal element (i.e. the smaller element). The equations of motion for the stationary seal element are easily obtained because the degrees-of-freedom are only coupled through fluid and contact forces and moments. These equations of motion, including static angular misalignment γ_{si} and inertial maneuver loads, are

$$I_{ts}\ddot{\gamma}_{s\xi} + D_s\dot{\gamma}_{s\xi} + K_s\gamma_{s\xi} = -I_{ts}\dot{\lambda}_p + K_s\gamma_{si,\xi} + M_{s\xi} + (M_{\mu s})_\xi \tag{78}$$

$$I_{ts}\ddot{\gamma}_{s\eta} + D_s\dot{\gamma}_{s\eta} + K_s\gamma_{s\eta} = -I_{ts}\dot{\lambda}_y + K_s\gamma_{si,\eta} + M_{s\eta} + (M_{\mu s})_\eta \tag{79}$$

$$m_s\ddot{u}_{sz} + D_{sz}\dot{u}_{sz} + K_{sz}u_{sz} = F_\zeta - F_{cls} - m_s(a_{O\zeta} + 2\lambda_p\dot{\epsilon}_{s\eta} - 2\lambda_y\dot{\epsilon}_{s\xi}) \tag{80}$$

$$m_s\ddot{\epsilon}_{s\xi} + D_{s\epsilon}\dot{\epsilon}_{s\xi} + K_{s\epsilon}\epsilon_{s\xi} = K_{s\epsilon}\epsilon_{si,\xi} + (F_{fs})_\xi + (F_{\mu s})_\xi - m_s(a_{O\xi} - 2\lambda_{ro}\dot{\epsilon}_{s\eta} + 2\lambda_y\dot{u}_{sz}) \tag{81}$$

$$m_s\ddot{\epsilon}_{s\eta} + D_{s\epsilon}\dot{\epsilon}_{s\eta} + K_{s\epsilon}\epsilon_{s\eta} = K_{s\epsilon}\epsilon_{si,\eta} + (F_{fs})_\eta + (F_{\mu s})_\eta - m_s(a_{O\eta} + g + 2\lambda_{ro}\dot{\epsilon}_{s\xi} - 2\lambda_p\dot{u}_{sz}) \tag{82}$$

where g is the acceleration due to gravity. The static misalignments $\gamma_{si,\xi}$, $\gamma_{si,\eta}$, $\epsilon_{si,\xi}$, and $\epsilon_{si,\eta}$ are imposed by applying forces and moments that enforce the misalignment. It must be noted once again that these equations of motion for the FMSR seal represent a generalized case of previous works, which considered simpler seal configurations such as the FMR or FMS. The equations of motion given here reduce to the forms derived in previous studies when the appropriate assumptions are instituted in the equations.

Thermal deformation: Viscous and frictional heating

Face coning in mechanical seals is typically generated by mechanical and thermal deformations. Mechanical deformations are small compared to thermal deformations and occur almost instantaneously.[26,38] Thermal deformations, on the other hand, are governed by dynamics which occur much slower than the seal dynamics. A complete model for thermoelastic deformation would require solving the elastic and heat conduction equations simultaneously with the proper boundary conditions. Fortunately, the thermoelastic dynamics of face coning can be accurately approximated in normal operating conditions by using the first-order model developed by Green.[26] This model relies on parameters obtained from a finite element simulation, and includes the appropriate heat transfer boundary conditions, thermoelastic deformations, and viscous heat generation

$$\tau_T\dot{\beta} + \beta = \beta_{ref}\left[\left(\frac{h_{ref}}{h_{mean}}\right)\left(\frac{\omega_r}{\omega_{ref}}\right)^2 + \frac{Q_f}{(Q_v)_{ref}}\right] \tag{83}$$

where β is the face coning and h_{mean} is the average film thickness across the sealing dam. The time scale is determined by the time constant τ_T, while the coning magnitude is controlled by the reference parameters β_{ref}, h_{ref}, and ω_{ref} found from the finite element simulation.[26] The frictional heat generation Q_f is normalized by the viscous heat generation at the reference parameters

$$Q_f = \int_0^{2\pi}\int_{r_i}^{r_o}\mu_f P_c(r,\theta)\omega_r r^2 \mathrm{d}r\mathrm{d}\theta \tag{84}$$

$$(Q_v)_{ref} = \int_0^{2\pi}\int_{r_i}^{r_o}\frac{\mu\omega_{ref}^2}{h_{ref}}r^3 \tag{85}$$

Importantly, the frictional heat generation is assumed to occur axisymmetrically even though the asperity contact is usually localized. This assumption is reasonable because of the time-scale discrepancy between the system dynamics and the thermoelastic deformations.[26] It should be noted that these thermoelastic deformation equations are provided for completeness, especially for future works, and are not simulated in this work.

System equations of motion

In matrix form, the equations of motion for the FMSR-ER system are

$$[M]\{\ddot{q}\} + ([D] + [\Lambda_1] + [G])\{\dot{q}\} + ([K] + [\Lambda_0] + [D_r])\{q\} = \bar{F}_a(\{q\},\{\dot{q}\},t) \tag{86}$$

where $[M]$ is the mass matrix, $[D]$ is the damping matrix, $[G]$ is the gyroscopic matrix, $[K]$ is the stiffness matrix, $[\Lambda]$ contains inertial forces due to maneuver rotation, and $[D_r]$ is the rotating damping matrix. The general vector of applied forces and moments, $\bar{F}_a$, is

given in equations (70) and (71). The mass matrix is

$$[M] = \begin{bmatrix} [M_s] & 0_{4\times4} \\ 0_{4\times4} & [M_r] \end{bmatrix},$$
$$[D] + [\Lambda_1] + [G] = \begin{bmatrix} [C_s] & 0_{4\times4} \\ 0_{4\times4} & [C_r] \end{bmatrix}, \quad (87)$$
$$[K] + [\Lambda_0] + [D_r] = \begin{bmatrix} [B_s] & 0_{4\times4} \\ 0_{4\times4} & [B_r] \end{bmatrix}$$

where

$$[M_s] = \begin{bmatrix} I_{ts} & 0 & 0 & 0 & 0 \\ & I_{ts} & 0 & 0 & 0 \\ & & m_s & 0 & 0 \\ & \text{sym.} & & m_s & 0 \\ & & & & m_s \end{bmatrix},$$
$$[M_r] = \begin{bmatrix} I_{tr} & 0 & 0 & 0 & -m_r d_r \\ & I_{tr} & 0 & m_r d_r & 0 \\ & & m_r & 0 & 0 \\ & \text{sym.} & & m_r & 0 \\ & & & & m_r \end{bmatrix} \quad (88)$$

$$[C_s] = \begin{bmatrix} D_s & 0 & 0 & 0 & 0 \\ & D_s & 0 & 0 & 0 \\ & & D_{sz} & -2m_s\lambda_y & 2m_s\lambda_p \\ & \text{skewsym.} & & D_{s\epsilon} & -2m_s\lambda_{ro} \\ & & & & D_{s\epsilon} \end{bmatrix},$$
$$[C_r] = \begin{bmatrix} D_r & I_{pr}\omega_r & 0 & 0 & 0 \\ & D_r & 0 & 0 & 0 \\ & & D_{rz} & -2m_r\lambda_y & 2m_r\lambda_p \\ & \text{skewsym.} & & D_{r\epsilon} & -2m_r\lambda_{ro} \\ & & & & D_{r\epsilon} \end{bmatrix} \quad (89)$$

$$[B_s] = \begin{bmatrix} K_s & 0 & 0 & 0 & 0 \\ & K_s & 0 & 0 & 0 \\ & & K_{sz} & 0 & 0 \\ & \text{sym.} & & K_{s\epsilon} & 0 \\ & & & & K_{s\epsilon} \end{bmatrix},$$
$$[B_r] = \begin{bmatrix} K_r - m_r a_{O\zeta} d_r & I_{pr}\dot{\omega}_r + \omega_r D_r & 0 & 0 & 0 \\ & K_r + m_r a_{O\zeta} d_r & 0 & 0 & 0 \\ & & K_{rz} & 0 & 0 \\ & \text{skewsym.} & & K_{r\epsilon} & 0 \\ & & & & K_{r\epsilon} \end{bmatrix} \quad (90)$$

Thermoelastic effects, given in equation (83), can be included in the above equations by appropriately expanding the state vector.

The complexity of the model presented above, in addition to that of the applied forces (fluid, contact, etc.), necessitates an iterative numeric solution of the system equations of motion. A closed-form analytic solution is perhaps available in some simplified situations (e.g. steady-state, no contact, and small motions about equilibrium). Still, addressing practical seal design problems in high-performance systems (e.g. hydrodynamic lift-off seals in high performance jet engines) almost certainly requires numeric solution due to the non-linear and complex nature of the problem. Specifics of applicable numeric methods are left to future works, where simulation results will also be provided.

Conclusions

Mechanical face seals are complicated systems, and correctly treating their dynamics requires amalgamating many disparate phenomena. In particular, mechanical face seals are constitutive to a larger turbomachine, which itself is constitutive to another system (e.g. an aircraft). For the first time, this work includes the effect of rotordynamics in the seal equations of motion, for a seal which is flexible in the axial, angular, and eccentric directions. The equations of motion are left in the generally transient form, where the shaft speed is free to remain a generic function of time to represent start-up, shut-down, or other transient modes of operation. In addition, and also for the first time, this work encapsulates the complex interaction of external accelerations and rotations (i.e. maneuver loads) with the dynamics of the face seal. A variety of excitations are considered here, including those which are natural to the system, such as fluid shear and normal fluid pressure, and those which represent seal faults (e.g. face contact, friction, dynamic angular misalignment, static angular misalignment, axial offset, and eccentric imbalance). The face coning, which is responsible for generating hydrostatic pressure between the seal faces, is left as a time-dependent function which depends on the thermoelastic deformation of the seal apparatus.

This novel and comprehensive mechanical face seal model represents a significant step forward in the state-of-the-art regarding non-contacting mechanical face seal dynamics. Now, the importance of coupled rotordynamic deflections on the performance and design of mechanical face seals can be assessed quantitatively. Furthermore, the impact of operating a mechanical face seal in a high-performance inertial maneuver environment can be assessed, and the conclusions applied to develop enhanced and refined mechanical face seals. Most importantly, the utility of the model presented here is that it has been left in the most general form possible in an effort to provide a tool that enjoys efficacy beyond simplified or assumed operating conditions. The model is also general enough that more advanced models for fluid pressure (e.g. compressible flow) or geometry (spiral-groove) can easily be substituted for the liquid-lubricated pressure profile given herein.

Declaration of Conflicting Interests

The author(s) declared no potential conflicts of interest with respect to the research, authorship, and/or publication of this article.

Funding

The author(s) received no financial support for the research, authorship, and/or publication of this article.

References

1. Etsion I. A review of mechanical face seal dynamics. *Shock Vibr Digest* 1982; 3: 9–14.
2. Lebeck AO. *Principles and design of mechanical face seals*. New York: Wiley Interscience, 1991.
3. Steinetz BM, Hendricks RC and Munson J. Advanced seal technology role in meeting next generation turbine engine goals. Technical report, National Aeronautics and Space Administration, Lewis Research Center, 1998.
4. Chupp RE, Hendricks RC, Lattime SB, et al. Sealing in turbomachinery. NASA, Technical Report 2006-214341, 1 August 2006.
5. Etsion I and Sharoni A. Performance of end-face seals with diametral tilt and coning – hydrostatic effects. *ASLE Trans* 1980; 23: 279–288.
6. Etsion I. Squeeze effects in radial face seals. *J Lubr Technol* 1980; 102: 145–151.
7. Sharoni A and Etsion I. Performance of end-face seals with diametral tilt and coning – hydrodynamic effects. *ASLE Trans* 1980; 24: 61–70.
8. Etsion I. The accuracy of the narrow seal approximation in analyzing radial face seals. *ASLE Trans* 1980; 22: 208–216.
9. Green I and Etsion I. Fluid film dynamic coefficients in mechanical face seals. *J Lubr Technol* 1983; 105: 297–302.
10. Etsion I. Dynamic analysis of noncontacting face seals. *J Tribol* 1982; 104: 460–468.
11. Green I and Etsion I. Nonlinear dynamic analysis of noncontacting coned-face mechanical seals. *ASLE Trans* 1986; 29: 383–393.
12. Green I. Gyroscopic and support effects on the steady-state response of a noncontacting flexibly-mounted rotor mechanical face seal. *J Tribol* 1989; 111: 200–208.
13. Green I. Gyroscopic and damping effects on the stability of a noncontacting flexibly-mounted rotor mechanical face seal. In: Kim JH and Yang W-J (ed.) *Proceedings of Second International Symposium on Transport Phenomena, Dynamics, and Design of Rotating Machinery*, Honolulu, Hawaii, Dynamics of Rotating Machinery, 1990, pp.153–173. New York: Hemisphere Publishing Company.
14. Green I. On the kinematic and kinetics of mechanical seals, rotors, and wobbling bodies. *Mech Mach Theor* 2008; 43: 909–917.
15. Lee AS and Green I. An experimental investigation of the steady-state response of a noncontacting flexibly mounted rotor mechanical face seal. *J Tribol* 1995; 117: 153–159.
16. Wileman J and Green I. The rotordynamic coefficients of mechanical seals having two flexibly mounted rotors. *J Tribol* 1991; 113: 795–804.
17. Wileman J and Green I. Steady-state analysis of mechanical seals with two flexibly mounted rotors. *J Tribol* 1997; 119: 200–204.
18. Wileman J and Green I. Parametric investigation of the steady-state response of a mechanical seal with two flexibly mounted rotors. *J Tribol* 1999; 121: 69–76.
19. Wileman J and Green I. The rotor dynamic coefficients of eccentric mechanical face seals. *J Tribol* 1996; 118: 215–224.
20. Wileman J. Dynamic response of eccentric face seals to synchronous shaft whirl. *J Tribol* 2004; 126: 301–309.
21. Etsion I and Sharoni A. The effect of coning on radial forces in misaligned radial face seals. *J Lubr Technol* 1980; 102: 139–144.
22. Etsion I and Constantinescu I. Experimental observation of the dynamic behavior of noncontacting coned-face mechanical seals. *ASLE Trans* 1984; 27: 263–270.
23. Lee AS and Green I. Higher harmonic oscillations in a non-contacting FMR mechanical face seal test rig. *J Vibr Acoust* 1994; 116: 161–167.
24. Varney P and Green I. Impact phenomena in a non-contacting mechanical face seal. *J Tribol* 2016; 139: 1–8.
25. Etsion I and Halperin G. A laser surface textured hydrostatic mechanical seal. *Tribol Trans* 2002; 45: 430–434.
26. Green I. A transient dynamic analysis of mechanical seals including asperity contact and face deformation. *Tribol Trans* 2002; 45: 284–293.
27. Wang CH, Soom A and Dargush GF. Transient thermoelastic contact of sliding rings with axisymmetric surface roughness. *J Tribol* 2004; 126: 217–224.
28. Valigi MC, Braccesi C and Logozzo S. A parametric study on friction instabilities in mechanical face seals. *Tribol Trans* 2016; 59: 911–922.
29. Lee AS and Green I. Rotordynamics of a mechanical face seal riding on a flexible shaft. *J Tribol* 1994; 116: 345–351.
30. Varney P and Green I. Analysis of intermittent rub in mechanical face seals. In: *STLE Annual Meeting*, Las Vegas, Nevada, 15–19 May 2016.
31. Green I. Effect of machine vibration on seal performance. In: *STLE Annual Meeting*, Las Vegas, Nevada, 15–19 May 2016.
32. Jackson RL and Green I. A finite element study of elasto-plastic hemispherical contact. *J Tribol* 2005; 127: 343–354.
33. Jackson RL and Green I. A statistical model of elasto-plastic asperity contact between rough surfaces. *Tribol Int* 2006; 39: 906–914.
34. Green I and Etsion I. A kinematic model for mechanical seals with antirotation locks or positive drive devices. *J Tribol* 1986; 108: 42–45.
35. Wileman JM. *Dynamic analysis of eccentric mechanical face seals*. PhD Thesis, Georgia Institute of Technology, 1994.
36. Varney P and Green I. Applying rough surface contact of curved conformal surfaces to rotor-stator rub. In: *STLE Annual Meeting*, Dallas, TX, 17–21 May 2015.
37. Varney P and Green I. Rough surface contact of curved conformal surfaces: an application to rotor-stator rub. *J Tribol* 2015; 138: 1–7.
38. Salant RF and Cao B. Unsteady analysis of a mechanical seal using Duhamel's method. *J Tribol* 2005; 127: 623–631.

Appendix

Notation

a_{Oi}	acceleration of point O in the ith direction.
C_o	axial centerline clearance between the seal elements.
d_r	axial offset of the rotating seal element.
D_i	secondary seal angular damping of body i.
D_{iz}	secondary seal axial damping of body i.
$D_{i\epsilon}$	secondary seal lateral damping of body i.
F_{spr}	secondary seal spring force.
h_i	film thickness at the inner seal radius.
h_o	film thickness at the outer seal radius.
I_{ti}	transverse mass moment of inertia of body i.
I_{pi}	polar mass moment of inertia of body i.
K_i	secondary seal angular stiffness of body i.
K_{iz}	secondary seal axial stiffness of body i.
$K_{i\epsilon}$	secondary seal lateral stiffness of body i.
m_i	mass of body i.
$P_c(r,\theta)$	contact pressure as a function of position.
P_i	inner seal pressure.
P_o	outer seal pressure.
r_b	balance radius of the seal faces.
r_i	inner radius of the seal faces.
r_o	outer radius of the seal faces.
u_{ij}	axial tilt of element i in the jth direction.
$\alpha(t)$	time-dependent shaft rotation angle.
β	seal face coning.
β_r	static phase angle of the rotating element imbalance.
γ_{ij}	angular tilt of element i in the jth direction.
γ^*	relative tilt.
γ_r	tilt angle of the rotating seal element.
γ_s	tilt angle of the stationary seal element.
λ_p	system pitch angular velocity.
λ_y	system yaw angular velocity.
λ_{ro}	system roll angular velocity.
μ	lubricant viscosity.
μ_f	coefficient of friction.
ψ_r	precession angle of the rotating seal element.
ψ_s	precession angle of the stationary seal element.
τ_T	thermal time constant.
χ	dynamic angular seal misalignment.
ω_r	shaft rotation rate.

Appendix 1. Components of the applied forces

The following equations provide specific component forms of the applied forces and moments acting on the rotating and stationary seal elements.

Fluid and contact pressure

$$M_{r\xi} = -\int_{r_i}^{r_o}\int_0^{2\pi} P(r,\theta) r^2 \sin\theta \mathrm{d}r\mathrm{d}\theta \tag{91}$$

$$M_{r\eta} = \int_{r_i}^{r_o}\int_0^{2\pi} P(r,\theta) r^2 \cos\theta \mathrm{d}r\mathrm{d}\theta \tag{92}$$

$$M_{s\xi} = \int_{r_i}^{r_o}\int_0^{2\pi} P(r,\theta)(r\sin\theta - \epsilon_\eta^*) r\mathrm{d}r\mathrm{d}\theta \tag{93}$$

$$M_{s\eta} = \int_{r_i}^{r_o}\int_0^{2\pi} P(r,\theta)(\epsilon_\xi^* - r\cos\theta) r\mathrm{d}r\mathrm{d}\theta \tag{94}$$

Fluid shear

$$(M_{fr})_\xi = \mu\omega_r \int_{r_i}^{r_o}\int_0^{2\pi} \frac{\gamma_{r\eta}\cos\theta - \gamma_{r\xi}\sin\theta}{h(r,\theta)} r^3 \cos\theta \mathrm{d}r\mathrm{d}\theta \tag{95}$$

$$(M_{fr})_\eta = \mu\omega_r \int_{r_i}^{r_o}\int_0^{2\pi} \frac{\gamma_{r\eta}\cos\theta - \gamma_{r\xi}\sin\theta}{h(r,\theta)} r^3 \sin\theta \mathrm{d}r\mathrm{d}\theta \tag{96}$$

$$(M_{fs})_\xi = -\mu\omega_r \int_{r_i}^{r_o}\int_0^{2\pi} \frac{\gamma_{s\eta}\cos\theta - \gamma_{s\xi}\sin\theta}{h(r,\theta)} r^3 \cos\theta \mathrm{d}r\mathrm{d}\theta \tag{97}$$

$$(M_{fs})_\eta = -\mu\omega_r \int_{r_i}^{r_o}\int_0^{2\pi} \frac{\gamma_{s\eta}\cos\theta - \gamma_{s\xi}\sin\theta}{h(r,\theta)} r^3 \sin\theta \mathrm{d}r\mathrm{d}\theta \tag{98}$$

Friction

Expanding equations (46) and (47), neglecting second-order terms, and ignoring moments about ζ gives the friction forces and moments caused by eccentricity and rotation

$$(F_{\mu r})_\xi = \mu_f \int_{r_i}^{r_o}\int_0^{2\pi} P_c(r,\theta)\left(\frac{-\dot{\epsilon}_\xi^* - r\omega_r\sin\theta}{\omega_r}\right)\mathrm{d}r\mathrm{d}\theta \tag{99}$$

$$(F_{\mu r})_\eta = \mu_f \int_{r_i}^{r_o} \int_0^{2\pi} P_c(r,\theta)\left(\frac{-\dot{\epsilon}_\eta^* + r\omega_r \cos\theta}{\omega_r}\right) \mathrm{d}r\mathrm{d}\theta \tag{100}$$

$$(F_{\mu s})_\xi = -(F_{\mu r})_\xi \tag{101}$$

$$(F_{\mu s})_\eta = -(F_{\mu r})_\eta \tag{102}$$

$$(M_{\mu r})_\xi = \mu_f \int_{r_i}^{r_o} \int_0^{2\pi} P_c(r,\theta) \times (\gamma_{r\eta}\cos\theta - \gamma_{r\xi}\sin\theta) r^2 \cos\theta \mathrm{d}r\mathrm{d}\theta \tag{103}$$

$$(M_{\mu r})_\eta = \mu_f \int_{r_i}^{r_o} \int_0^{2\pi} P_c(r,\theta) \times (\gamma_{r\eta}\cos\theta - \gamma_{r\xi}\sin\theta) r^2 \sin\theta \mathrm{d}r\mathrm{d}\theta \tag{104}$$

$$(M_{\mu s})_\xi = -\mu_f \int_{r_i}^{r_o} \int_0^{2\pi} P_c(r,\theta) \times (\gamma_{s\eta}\cos\theta - \gamma_{s\xi}\sin\theta) r^2 \cos\theta \mathrm{d}r\mathrm{d}\theta \tag{105}$$

$$(M_{\mu s})_\eta = -\mu_f \int_{r_i}^{r_o} \int_0^{2\pi} P_c(r,\theta) \times (\gamma_{s\eta}\cos\theta - \gamma_{s\xi}\sin\theta) r^2 \sin\theta \mathrm{d}r\mathrm{d}\theta \tag{106}$$